Remote Sensing of Environment 152 (2014) 1–14

Contents lists available at ScienceDirect

Remote Sensing of Environment

journal homepage: www.elsevier.com/locate/rse

Sensitivity of vegetation indices and gross primary production of tallgrass prairie to severe drought

Pradeep Wagle [a], Xiangming Xiao [a,*], Margaret S. Torn [b], David R. Cook [c], Roser Matamala [c], Marc L. Fischer [b], Cui Jin [a], Jinwei Dong [a], Chandrashekhar Biradar [d]

[a] Department of Microbiology and Plant Biology, Center for Spatial Analysis, University of Oklahoma, Norman, OK 73019, USA
[b] Atmospheric Science Department, Lawrence Berkeley National Laboratory, Berkeley, CA 94720, USA
[c] Argonne National Laboratory, Argonne, IL 60439, USA
[d] International Center for Agricultural Research in Dry Areas (ICARDA), Amman, Jordan

ARTICLE INFO

Article history:
Received 5 February 2014
Received in revised form 16 May 2014
Accepted 16 May 2014
Available online xxxx

Keywords:
Drought
Gross primary production
Light use efficiency
MODIS
Vegetation Photosynthesis Model (VPM)

ABSTRACT

Drought affects vegetation photosynthesis and growth. Many studies have used the normalized difference vegetation index (NDVI), which is calculated as the normalized ratio between near infrared and red spectral bands in satellite images, to evaluate the response of vegetation to drought. In this study, we examined the impacts of drought on three vegetation indices (NDVI, enhanced vegetation index, EVI, and land surface water index, LSWI) and CO_2 flux from three tallgrass prairie eddy flux tower sites in the U.S. Gross primary production (GPP) was also modeled using a satellite-based Vegetation Photosynthesis Model (VPM), and the modeled GPP (GPP_{VPM}) was compared with the GPP (GPP_{EC}) derived from eddy covariance measurements. Precipitation at two sites in Oklahoma was 30% below the historical mean in both years of the study period (2005–2006), while the site in Illinois did not experience drought in the 2005–2007 study period. The EVI explained the seasonal dynamics of GPP better than did NDVI. The LSWI dropped below zero during severe droughts in the growing season, showing its potential to track drought. The result shows that GPP was more sensitive to drought than were vegetation indices, and EVI and LSWI were more sensitive than NDVI. We developed a modified function (W_{scalar}), calculated as a function of LSWI, to account for the effect of severe droughts on GPP in VPM. The GPP_{VPM} from the modified VPM accounted for the rapid reduction in GPP during severe droughts and the seasonal dynamics of GPP_{VPM} agreed reasonably well with GPP_{EC}. Our analysis shows that 8-day averaged values (temperature, vapor-pressure deficit) do not reflect the short-term extreme climate events well, suggesting that satellite-based models may need to be run at daily or hourly scales, especially under unfavorable climatic conditions.

1. Introduction

More accurate quantification of carbon fluxes across regions, continents, or the globe is necessary for a better understanding of feedbacks between terrestrial ecosystems and the atmosphere (Peters et al., 2007). Eddy covariance (EC) systems are considered one of the most accurate micrometeorological methods at field scales. The EC systems provide continuous measurements of net ecosystem CO_2 exchange (NEE, the balance between gross primary production, GPP, and ecosystem respiration, ER). The EC-measured NEE is separated into two major components: GPP and ER using different modeling approaches (Reichstein et al., 2005), and GPP can be used to quantify crop productivity and to understand temporal variability in productivity (Falge et al., 2002). Moreover, accurate information on GPP and NEE of terrestrial ecosystems is of great importance for monitoring changes in the atmospheric CO_2 concentration (Baldocchi et al., 2001). As a result, the number of EC sites has increased in recent years. However, EC provides integrated carbon flux measurements only at the scale of the tower footprints, with longitudinal dimensions ranging from a hundred meters to several kilometers, depending on the height of the tower and vegetation, and the homogeneity of the fetch (Schmid, 1994). Additionally, EC measurements are difficult to interpret in heterogeneous or complex terrain (Running et al., 1999). Further, the logistical requirements and cost of EC systems prohibit extensive installation, leaving much of the world unsampled. These challenges necessitate scaling-up EC observations to regional or continental scales to examine terrestrial carbon cycling over large areas (Xiao et al., 2008). One approach to regional extrapolation of site-specific flux measurements is to use satellite observations and climate data (Turner et al., 2003; Xiao et al., 2004). Consistent, repetitive, and systematic observations of vegetation dynamics and ecosystems from satellite remote sensing allow us to characterize vegetation structure and to estimate GPP or net primary production (NPP) of ecosystems (Field, Randerson, & Malmström, 1995; Potter et al., 1993; Ruimy, Saugier, & Dedieu, 1994). The Moderate Resolution Imaging

* Corresponding author at: Center for Spatial Analysis, University of Oklahoma, USA. Tel.: +1 405 325 8941.
E-mail address: xiangming.xiao@ou.edu (X. Xiao).

http://dx.doi.org/10.1016/j.rse.2014.05.010
0034-4257/

Spectroradiometers (MODIS) on board the NASA's Terra and Aqua satellites provide global estimates of 8-day GPP at 1 km spatial resolution, which is compatible with the footprint sizes of EC systems. Thus, many EC sites provide GPP estimates with relevance for validating MODIS products (Turner et al., 2003). Recently, several studies have used satellite remote sensing data to upscale EC measurements to quantify GPP over large areas (Alfieri et al. 2009; Beer et al., 2010; Papale & Valentini, 2003; Wu, Chen, & Huang, 2011; Wu, Gonsamo, Zhang, & Chen, 2014; Xiao et al., 2010; Xiao, Hollinger, et al., 2004; Yamaji et al., 2008).

Satellite-based production efficiency models (PEMs) employ the product of the absorbed photosynthetically active radiation (APAR) and the light-use efficiency (LUE) to estimate GPP (Monteith, 1972; Potter et al., 1993). Most of these PEMs consider fraction of APAR as a linear function of normalized difference vegetation index (NDVI) (Tucker, 1979), which is a normalized ratio between red and near-infrared (ρ) bands, as defined below:

$$NDVI = \frac{\rho_{nir} - \rho_{red}}{\rho_{nir} + \rho_{red}}. \tag{1}$$

However, NDVI has been reported to be sensitive to atmospheric conditions, soil background, and saturation in multilayered and closed canopies (Huete, Liu, Batchily, & Van Leeuwen, 1997). Thus, vegetation photosynthesis model (VPM), a satellite-based PEM, uses the enhanced vegetation index (EVI) as a function of fraction of APAR instead of NDVI (Xiao, Hollinger, et al., 2004). The EVI employs an additional blue band for atmospheric correction and is calculated from blue, red, and near-infrared bands (Huete et al., 1997) as follows:

$$EVI = G \times \frac{\rho_{nir} - \rho_{red}}{\rho_{nir} + (C_1 \times \rho_{red} - C_2 \times \rho_{blue}) + L} \tag{2}$$

where G (2.5) is the gain factor, C_1 (6) and C_2 (7.5) are band-specific atmospheric resistance correction coefficients, and L (1) is a background brightness correction factor. VPM also uses land surface water index (LSWI), which is calculated as the normalized difference between NIR (0.78–0.89 μm) and SWIR (1.58–1.75 μm) spectral bands, as follows (Xiao, Boles, Liu, Zhuang, & Liu, 2002):

$$LSWI = \frac{\rho_{nir} - \rho_{swir}}{\rho_{nir} + \rho_{swir}}. \tag{3}$$

The potential of VPM for scaling-up GPP has been tested in temperate, boreal, and moist tropical evergreen forests (Xiao, Hollinger, et al., 2004; Xiao, Zhang, Hollinger, Aber, & Moore, 2005; Xiao et al., 2005; Xiao et al., 2004), savanna woodlands (Jin et al., 2013), alpine ecosystems (Li et al., 2007), a temperate grassland in Central Asia (Wu et al., 2008), and corn (*Zea mays* L.) fields (Kalfas, Xiao, Vanegas, Verma, & Suyker, 2011; Wang, Xiao, & Yan, 2010). However, this approach has not been applied to the native grasslands, or prairie, of North America. Prairie grasslands experience grazing, burning, and extreme climate events like drought. However, EC studies over prairie have been reported only at a very few sites (Fischer et al., 2012; Suyker, Verma, & Burba, 2003; Verma, Kim, & Clement, 1989). Accurate estimation of the spatial and temporal patterns of GPP in grasslands at large spatial scales is necessary to improve our understanding of the effects of fire and extreme climatic events on these ecosystems (Fischer et al., 2012).

In this study, we tested VPM's estimation of GPP for two tallgrass prairie ecosystems in Oklahoma and one in Illinois, for multiple years, by integrating the MODIS images (8-day surface reflectance) and climate variables acquired from EC measurements. These study sites had diverse climatic conditions during the study. The site in Illinois had good rainfall during the study period (2005–2007), while precipitation at the Oklahoma sites was 30% below the historical mean for both years (2005–2006) of the study period. As a result, soil moisture at the Oklahoma sites gradually declined, from more productive conditions in 2005 to dry and less productive conditions by summer 2006 (Fischer et al., 2012). This change provided a useful opportunity to evaluate VPM's capability for estimating GPP under severe drought conditions. Thus, the major objectives of this study were to estimate the seasonal dynamics and interannual variations in GPP within tallgrass prairie, using VPM and to evaluate the response of vegetation indices (EVI, NDVI, and LSWI) and GPP to drought conditions.

2. Materials and methods

2.1. Site description

2.1.1. The El Reno sites in Oklahoma

Two study sites [control (35.5465°N, −98.0401°W, 423 m asl) and burned sites (35.5497°N, −98.0402°W, 423 m asl)] are located in two adjacent 33 ha pastures at the United States Department of Agriculture—Agricultural Research Service (USDA-ARS) Grazing Lands Research Laboratory (GRL) in El Reno, Oklahoma. The landscape features of the sites are shown in Fig. 1; an overview of the study sites is presented in Table 1. Both pastures were not burned after 1990 and they were grazed at equal, moderate stocking rates through the 2000 growing season. One site was burned on March 09, 2005; the other plot was left unburned. Dominant species at these sites are big bluestem (*Andropogon gerardi* Vitman), little bluestem (*Schizachyrium halapense* (Michx.) Nash.), and other grasses common to tallgrass prairie ecosystems. Detailed descriptions of the sites can be found in Fischer et al. (2012).

2.1.2. The Fermi site in Illinois

The third study site, a restored prairie in Illinois (41.8406°N, −88.2410°W, 226 m asl), was farmed for more than 100 years and then converted to prairie in 1989. The site is dominated by C_4 grasses and forbs. Detailed descriptions of the site can be found on the AmeriFlux website (http://ameriflux.ornl.gov/fullsiteinfo.php?sid=47). The landscape features of the site are shown in Fig. 1; a site overview is presented in Table 1. Because of the marginal fetch to the east, the MODIS pixel included adjacent land parcels (Fig. 1). Immediately east of the prairie is a strip of corn/soybean (*Glycine max* L.) rotation, while just to the east of that is native grassland (distinct from prairie).

2.2. Eddy flux data and site-specific meteorological data

Site-specific climate and Level-4 CO_2 flux data for the study sites were acquired from the AmeriFlux website (http://ameriflux.ornl.gov/). The Level-4 data consists of CO_2 flux (NEE and GPP) with four different time steps: half-hourly, daily, 8-day, and monthly. These data were gap-filled using the Marginal Distribution Sampling (MDS) method (Reichstein et al., 2005). We used two years of data (2005 and 2006) for the El Reno sites (AMF_USARc and AMF_USARb) and three years of data (2005–2007) for the Fermi site (AMF_USIB2). Eight-day GPP data (g C m^{-2} day^{-1}) were compared with composite intervals of MODIS data. Because the EC system does not measure GPP directly, the GPP is estimated as:

$$GPP = ER_d - NEE_d \tag{4}$$

where ER_d is daytime ecosystem respiration and NEE_d is daytime NEE.

The 8-day Level-4 datasets also contain air temperature, precipitation, PAR, and soil water content. Seasonal dynamics and interannual variations of PAR, mean air temperature, soil water content, and precipitation at all study sites are presented in Fig. 2.

2.3. Satellite data

As part of the NASA Earth Observing System, MODIS scans the entire surface of the earth every 1–2 days and acquires data in 36 spectral

Fig. 1. Landscapes of three eddy flux sites. The red boarder line corresponds to the size of one MODIS pixel at 500-m spatial resolution, and the red dot represents the location of the flux tower.

bands. Seven spectral bands are designed for the vegetation and land-surface studies. These bands are blue (459–479 nm), green (545–565 nm), red (620–670 nm), near infrared (NIR1: 841–875 nm, NIR2: 1230–1250 nm), and shortwave infrared (SWIR1: 1628–1652 nm, SWIR2: 2105–2155 nm). Among them, we used the blue, green, red, NIR1, and SWIR1 bands to derive the spectral indices (EVI, NDVI, and LSWI). The 8-day composite images are available at spatial resolutions of 250 m (red and NIR1) and 500 m (blue, green, NIR2, SWIR1, and SWIR2). Forty-six 8-day composite images are available in a year, beginning with January 1st. Time series MOD09A1 data for one MODIS pixel (500 m × 500 m), where a flux tower is located, were downloaded from the MODIS data portal at the Earth Observation and Modeling Facility (EOMF), University of Oklahoma (http://eomf.ou.edu/visualization/gmap/). Three vegetation indices – NDVI, EVI, and LSWI – for each MODIS 8-day composite were calculated according to Eqs. (1), (2), and (3), respectively.

2.4. Description of VPM and parameter estimation

Xiao, Hollinger, et al. (2004), Xiao, Zhang, et al. (2004) developed a satellite-based VPM that is different from the model used in the MODIS-GPP ($GPP_{MOD17A2}$) product. VPM estimates GPP based on the conceptual partitioning of vegetation canopies into nonphotosynthetic vegetation (npv) and photosynthetically active vegetation (pav) or chlorophyll (chl).

$$FAPAR_{canopy} = FAPAR_{chl} + FAPAR_{npv} \tag{5}$$

where $FAPAR_{CANOPY}$ is the fraction of PAR absorbed by the canopy, $FAPAR_{chl}$ is the fraction of PAR absorbed by chlorophyll, and $FAPAR_{npv}$ is the fraction of PAR absorbed by nonphotosynthetic vegetation. $FAPAR_{canopy}$ is generally estimated as a linear or nonlinear function of NDVI (Prince & Goward, 1995; Ruimy et al., 1994):

$$FAPAR_{canopy} = a + b \times NDVI \tag{6}$$

where a and b are empirical constants. $FAPAR_{canopy}$ has also been computed as a function of leaf area index (LAI) and a light extinction coefficient (k) (Ruimy, Kergoat, & Bondeau, 1999).

$$FAPAR_{canopy} = 0.95\left(1 - e^{-k \times LAI}\right) \tag{7}$$

However, in VPM, $FAPAR_{chl}$ is estimated as a linear function of EVI as given in Eq. (8) where the coefficient α is set to 1.0 (Xiao, Hollinger, et al., 2004).

$$FAPAR_{chl} = \alpha \times EVI \tag{8}$$

In VPM, GPP is computed as follows:

$$GPP = \varepsilon_g \times FAPAR_{chl} \times PAR \tag{9}$$

where ε_g is the light-use efficiency [LUE, g C mol^{-1} photosynthetic photon flux density (PPFD)] which is reduced by nonoptimal temperature or water stress:

$$\varepsilon_g = \varepsilon_0 \times T_{scalar} \times W_{scalar} \tag{10}$$

where ε_0 is the apparent quantum yield or maximum light-use efficiency (g C mol^{-1} PPFD), and T_{scalar} and W_{scalar} are the down-regulation scalars (ranging between 0 and 1) to account for the effects of temperature and water stress on the LUE, respectively.

The site-specific ε_0 can be obtained from the analysis of the NEE–PPFD relationship at eddy flux tower sites or can be obtained from a survey of the literature (Ruimy, Jarvis, Baldocchi, & Saugier, 1995). In this study, the ε_0 value was estimated using the following rectangular hyperbolic light-response function (NEE–PPFD relationship):

$$NEE = \frac{\varepsilon_0 \times GPP_{max} \times PPFD}{\varepsilon_0 \times PPFD + GPP_{max}} + ER \tag{11}$$

where GPP_{max} is the maximum canopy CO_2 uptake rate (μmol m^{-2} s^{-1}) at light saturation, and ER is respiration rate. We fit Eq. (11) using half hourly NEE and PPFD data, as shown in Fig. 3, for a one-week period during peak growth. The largest observed ε_0 value was 0.062 ± 0.0066 (standard error) mol CO_2 mol^{-1} PPFD at the Fermi site during the week June 24–30, 2007. The El Reno grasslands experienced drought in both years of the study period; the site received 600 ± 20 mm and 620 ± 20 mm annual precipitation in 2005 and 2006, respectively, while the average annual precipitation (1971–2000) for the site was 860 mm. As a result, smaller ε_0 values were observed at the El Reno sites. The highest observed ε_0 values were 0.035 ± 0.0018 mol CO_2 mol^{-1} PPFD (July 8–15, 2005) at the El Reno control site and 0.026 ± 0.001 mol CO_2 mol^{-1} PPFD (June 24–31, 2005) at

Table 1
Overview of the study sites.

Site code	Site name	Lat, lon (flux tower)	Data used	Field size (ha)	Dominant species	References
US-ARc	El Reno control (Oklahoma)	35.5465 −98.0401	2005–2006	33	Big bluestem, little bluestem	Fischer et al. (2012)
US-ARb	El Reno burned (Oklahoma)	35.5497 −98.0402	2005–2006	33	Big bluestem, little bluestem	Fischer et al. (2012)
US-IB2	Fermi Prairie (Illinois)	41.8406 −88.2410	2005–2007	26	C_4 grasses and forbs	

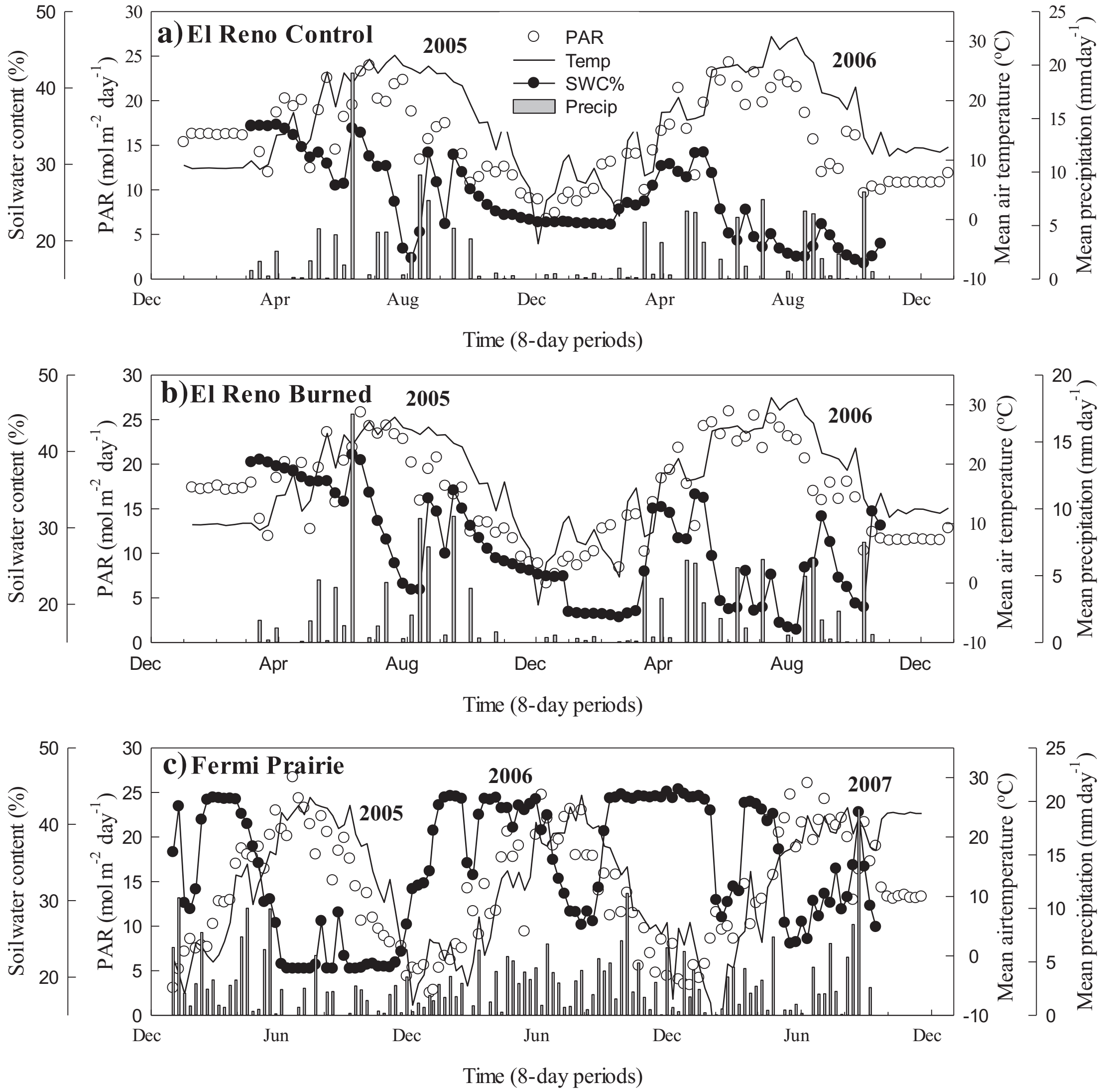

Fig. 2. Seasonal dynamics and interannual variations of photosynthetically active radiation (PAR), mean air temperature, soil water content (SWC in percentage), and precipitation at three tallgrass prairie sites. Each data point represents an average value of 8-day composites.

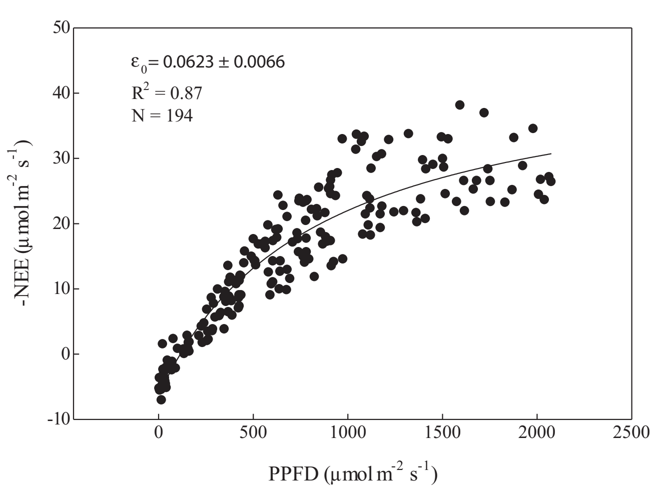

Fig. 3. Light–response curve function for a selected time period (June 24–31, 2007) at the Fermi site. Each data point is a 30-minute daytime net ecosystem CO_2 exchange (NEE) value from tower measurements, PPFD is photosynthetic photon flux density, ε_0 is the apparent quantum yield [the initial slope of the light response curve (mol CO_2 mol^{-1} of photon)], R^2 is the coefficient of determination, and N represents the number of data points.

the El Reno burned site. Thus, we selected the upper limit of the highest ε_0 ($0.062 + 1.96 \times 0.0066 = 0.075$ mol CO_2 mol^{-1} PPFD or 0.9 g C mol^{-1} PPFD) observed for the Fermi site as a maximum ε_0, and this single value was used to model GPP across all site-years.

T_{scalar} was estimated at each time step as in Terrestrial Ecosystem Model (TEM) (Raich et al., 1991):

$$T_{scalar} = \frac{(T - T_{min})(T - T_{max})}{\left[(T - T_{min})(T - T_{max}) - \left(T - T_{opt}\right)\right]^2} \tag{12}$$

where T_{min}, T_{max}, and T_{opt} are minimum, maximum, and optimal temperatures (°C) for photosynthetic activity, respectively. The temperature range for photosynthesis is quite large. We sorted GPP for the active growing season (May–August) over study periods for all three sites separately to 11 different temperature classes at a range of 3 °C difference (<9, 9–12, 12–15, 15–18, 18–21, 21–24, 24–27, 27–30, 30–33, 33–36, and >36 °C), and computed mean temperature and GPP for each temperature bin. From our analysis, T_{opt} was around 30 °C for all three sites (Fig. 4). In this study, T_{min} and T_{max} were set to −1 and 50 °C, respectively.

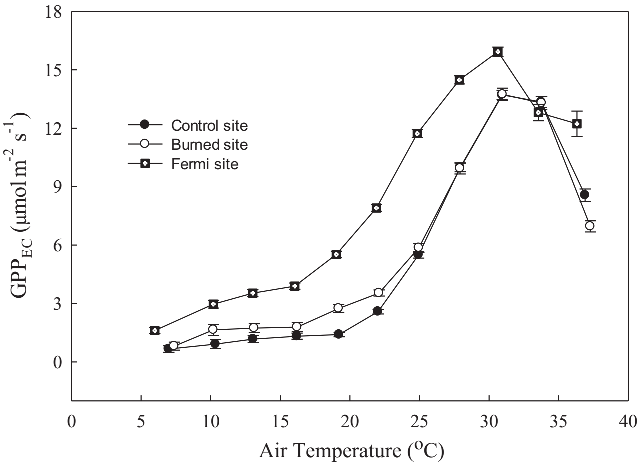

Fig. 4. Response of gross primary production (GPP_{EC}) to air temperature. Each data point is mean GPP_{EC} during the active growing season (May–August) over the study period for each temperature class. Bars represent standard errors of the means.

The LSWI increases at the beginning of the growing season and declines with plant senescence, resulting in positive values during the active growing period (Fig. 5). However, LSWI values dropped below zero even during the active growing period in 2006 at both El Reno sites, owing to severe drought (Fig. 5). To better characterize the seasonal evolution of LSWI at these sites, we acquired MODIS-derived LSWI values for 13 years (2000–2013) and plotted the mean seasonal cycle of LSWI (Fig. 6). Fig. 6 shows that long-term mean LSWI values were consistently larger than zero (positive) from May to September (growing season for grasses), but LSWI values in dry periods of the 2006 growing season were negative. Based on this observation, we proposed two different approaches of W_{scalar} calculation for the normal (LSWI > 0) and drought (LSWI < 0) conditions during the growing season (May to September). For normal periods, the seasonal dynamics of W_{scalar} were estimated using the following approach:

$$W_{scalar} = \frac{1 + LSWI}{1 + LSWI_{max}} \tag{13}$$

where $LSWI_{max}$ represents the maximum LSWI within the plant growing season. We calculated the mean seasonal cycle of LSWI over the study period and then selected the maximum mean LSWI within the plant growing season as an estimate of $LSWI_{max}$ as in Xiao, Hollinger, et al. (2004). During 2005–2006, the $LSWI_{max}$ value was 0.176 for the El Reno control site and 0.16 for the El Reno burned site. During 2005–2007, the $LSWI_{max}$ value was 0.29 for the Fermi site.

For drought periods, we suggested a modified W_{scalar} estimation approach as follows:

$$W_{scalar} = \text{long-term } LSWI_{\max} + LSWI. \tag{14}$$

In this study, a maximum value of LSWI observed during the 2000–2013 growing seasons was used as a long-term $LSWI_{max}$. Those values were 0.39 for the El Reno control site and 0.40 for the El Reno burned site. Our proposed approach is similar to the one ($W_{scalar} = 0.5 +$ LSWI) proposed by He et al. (2014) for simulation of the rapid response of carbon assimilation to water availability regardless of water condition during the entire year. We proposed to replace 0.5 with a site-specific long-term $LSWI_{max}$, which helps measure a deviation from the normal condition. Taking a value of LSWI (−0.06) at the El Reno control site on August 5th 2006 as an example, Eq. (13) yielded a W_{scalar} value of 0.80, which did not reflect a severe drought condition as W_{scalar} ranges from 0 to 1. As a result, the model overestimated GPP substantially during droughts. The modified approach of W_{scalar} provided a value of 0.33 (Eq. (14)) and accounted for the rapid reduction in GPP during the severe water stress.

2.5. VPM model performance evaluation

Tower-estimated (GPP_{EC}) and VPM-modeled GPP (GPP_{VPM}) values were compared to assess the validity of the model. A linear regression model was developed between 8-day composite GPP_{EC} and GPP_{VPM} values. To evaluate the model agreement, three statistics RMSE (root mean squared error), MAE (mean absolute error), and R^2 (coefficient of determination) values were used. Values of RMSE and MAE were calculated as follows:

$$RMSE = \sqrt{\frac{\sum_i^j (GPP_{EC} - GPP_{VPM})^2}{j}} \tag{15}$$

$$MAE = \left[\frac{\left(\sum_i^j |GPP_{EC} - GPP_{VRM}|\right)}{j}\right] \tag{16}$$

where j is the total number of observations.

2.6. A comparison with the standard MODIS-GPP product (MOD17A2)

The MODIS Land Science Team provides the standard MODIS-GPP/NPP product (MOD17A2) to the public (Running, Nemani, Glassy, & Thornton, 1999). MODIS-GPP ($GPP_{MOD17A2}$) is computed as follows:

$$GPP_{MOD17A2} = \varepsilon \times FPAR_{canopy} \times PAR \tag{17}$$

where ε is the light use efficiency, $FPAR_{canopy}$ is the fraction of PAR absorbed by the canopy and PAR is the photosynthetically active radiation. $FPAR_{canopy}$ is derived from the standard FPAR and leaf area index (LAI) product (MOD15A2) generated by the MODIS Land Science Team (Myneni et al., 2002).

MOD17A2 and MOD15A2 data for the El Reno sites were downloaded from the MODIS data portal at the Earth Observation and Modeling Facility (EOMF), University of Oklahoma (http://eomf.ou.edu/visualization/gmap/). These global datasets are available from 2000 to the present at 1 km spatial resolution and 8-day temporal resolution. But the $GPP_{MOD17A2}$ data were unavailable for the Fermi site when data files were downloaded from two different data sources: the University of Oklahoma, EOMF website (http://eomf.ou.edu/visualization/gmap/) and the Oak Ridge National Laboratory Distributed Active Archive Center (ORNL DAAC) website (http://daac.ornl.gov/MODIS/modis.html).

3. Results

3.1. Seasonal dynamics of climate

Because the study sites at El Reno were located in two adjacent plots, we can see highly similar seasonal dynamics for PAR, temperature, soil water content, and precipitation (Fig. 2). Fig. 2 shows that the 2006 growing season was warmer and exceptionally drier compared with the 2005 growing season; 8-day average air temperature reached a maximum of about 28 °C in 2005 and about 31 °C in 2006 at both the control and burned sites. In 2005, volumetric soil water content ranged from 18% to 35% at the control site and 22% to 40% at the burned site. The higher soil–water content at the burned site may be due to the higher soil organic matter content in that field. In 2006, soil–water content ranged between 17% and 32% at the control site and between 17% and 34% at the burned site. The maximum PAR during the growing season reached up to 24–26 mol m^{-2} day^{-1} at these sites.

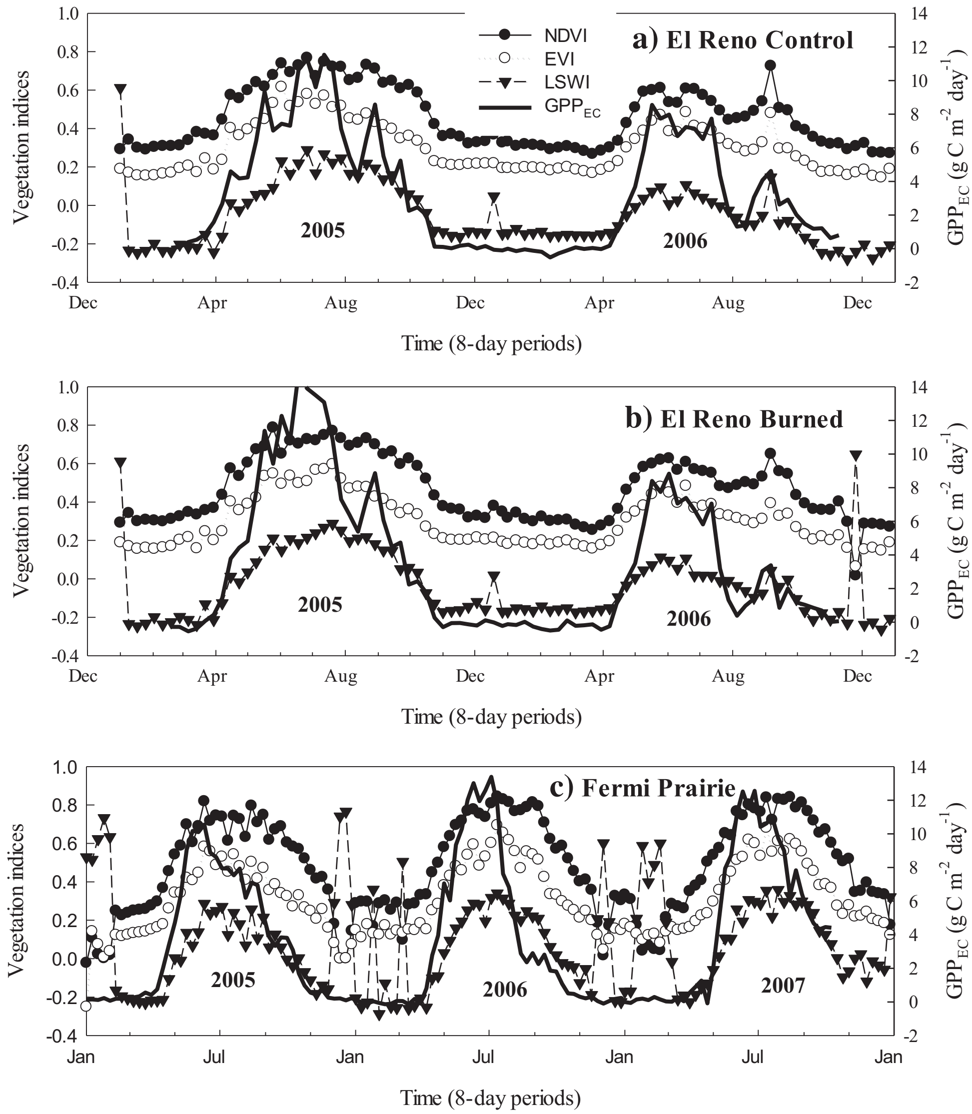

Fig. 5. Seasonal and interannual variations in observed gross primary production (*GPP*$_{EC}$) and MODIS-derived vegetation indices (NDVI, EVI, and LSWI) at three flux sites.

The Fermi site received good rainfall throughout entire study period (2005–2007) (Fig. 2). However, the 2005 growing season was relatively warmer and drier compared to those of 2006 and 2007 (Fig. 2). The range of volumetric soil water content was 21–43% in 2005, 27–44% in 2006, and 24–44% in 2007; 8-day average air temperature reached peak values of 25–27 °C. The PAR reached peak values of 26–27 mol m^{-2} day^{-1}.

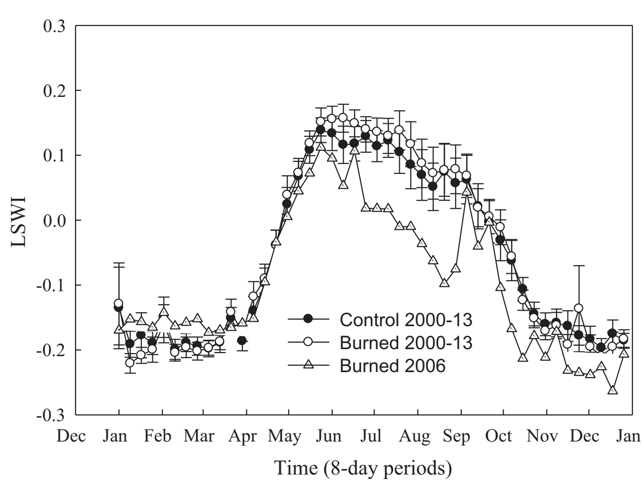

Fig. 6. Seasonal evolution of MODIS-derived land surface water index (LSWI) at the El Reno sites. Bars represent standard errors of the means.

3.2. Seasonality of GPP and vegetation indices

The seasonal dynamics of GPP followed the same patterns at all three tower sites (Fig. 5). GPP started to rise (>1 g C m^{-2} day^{-1}) at the beginning of April, reached a maximum during June–July, and then started to decline, falling below 1 g C m^{-2} day^{-1} at the end of October. This suggests that the prairie vegetation greened up in April and entered into a senescence phase by the end of October. This finding is well supported by the patterns of MODIS-derived vegetation indices as well (Fig. 5). NDVI, EVI, and LSWI started to increase with the beginning of the plant growing season, and started to decline with the beginning of senescence, which corresponded with the increase and decrease of GPP. However, some spikes in LSWI were observed in winter because of snow cover. Similar to GPP, the vegetation indices also reached peak values during the active growth phase (June–July). This suggests that these vegetation indices are good indicators for identifying plant phenology. In the following, we discuss the seasonality of GPP and vegetation indices for individual sites separately.

3.2.1. The El Reno control site

At this site, GPP was above 1 g C m^{-2} day^{-1} for six and half months each year, from the beginning of April to mid-October 2005 and from mid-April to the end of October 2006. Vegetation indices showed similar patterns, with higher values from April to October. The thresholds of NDVI, EVI, and LSWI for the periods of GPP > 1 g C m^{-2} day^{-1} were >0.35, >0.20, and >−0.16, respectively in 2005, and >0.30, >0.20, and >−0.20, respectively in 2006. The maximum GPP (11.5 g C m^{-2} day^{-1}) was observed in mid-July 2005, while the EVI was about 0.57. The maximum EVI of 0.62 was observed in the first week of June 2005. Similarly, the NDVI reached a maximum (0.77) at the end of June 2005. In 2006, maximum GPP was lower (~8 g C m^{-2} day^{-1}) than in 2005, and it occurred from mid-May to early June. The maximum EVI in 2006 was about 0.48; the maximum NDVI was 0.73 in mid-June.

3.2.2. The El Reno burned site

At this site, GPP was above 1 g C m^{-2} day^{-1} from the first week of April to mid-October 2005 and a slightly shorter period, from mid-April to the first week of October 2006. The thresholds of NDVI, EVI, and LSWI for the periods of GPP > 1 g C m^{-2} day^{-1} were >0.43, >0.23, and >−0.12, respectively, in 2005, and >0.36, >0.23, and >−0.15, respectively, in 2006. In 2005, the maximum GPP (14.9 g C m^{-2} day^{-1}) was observed during the third week of June when EVI was ~0.50. The maximum EVI (0.6) and NDVI (0.77) were observed in the third week of July 2005. Similar to the control site, maximum GPP was lower (8.8 g C m^{-2} day^{-1}) at this site in 2006 than in 2005; and earlier, with the maximum occurring in the first week of June, when EVI was about 0.45. The maximum EVI in 2006 was 0.48, and the NDVI was 0.62 in the last week of May.

3.2.3. The Fermi site

GPP was above 1 g C m^{-2} day^{-1} for about six months, starting from mid-April to mid-October, in all three years (2005–2007). However, GPP declined very rapidly after July 2006 (Fig. 7). The drastic difference in GPP pattern in 2006 compared to 2005 and 2007 was a result of an infestation of white sweet clover (*Melilotus alba*) that dominated the field. It died out completely by the end of July 2006, leaving very little green vegetation after that, and resulting in the field being a carbon source through the remainder of the growing season. The thresholds of NDVI, EVI, and LSWI for the periods of GPP > 1 g C m^{-2} day^{-1} were >0.36, >0.17, and >−0.21, respectively in 2005, and >0.44, >0.25, and >−0.10, respectively in 2006, and >0.40, >0.22, and >−0.14, respectively in 2007. The maximum GPP (10.6 g C m^{-2} day^{-1}) in 2005 occurred during the second week of June, when the maximum EVI (0.58) and NDVI (0.82) were observed. In 2006, the maximum GPP of 13.4 g C m^{-2} day^{-1} was observed during the first week of July, when EVI was 0.60. The EVI reached a maximum (0.69) in July's second week, and the NDVI reached a peak (0.88) in July's third week in 2006. The maximum GPP in 2007 was 12.6 g C m^{-2} day^{-1} in the last week of June, when EVI was ~0.60. The maximum EVI was 0.68, and the NDVI was 0.84 in the second week of July.

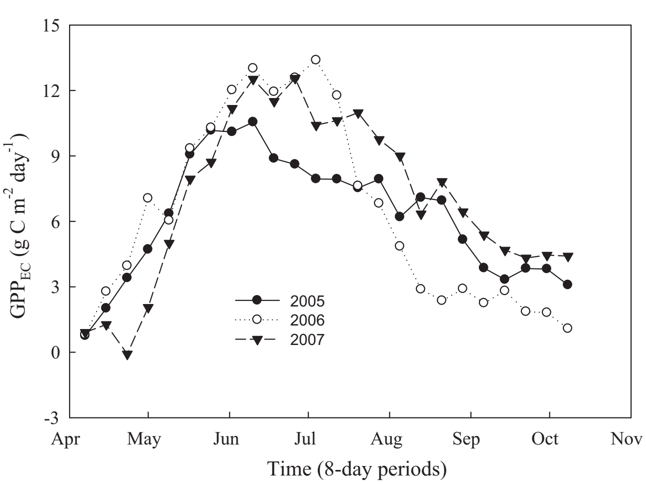

Fig. 7. Seasonal patterns of gross primary production (GPP_{EC}) at the Fermi site. Data points represent 8-day composite average values.

3.3. Relationship between GPP_{EC} and vegetation indices

Relationships between vegetation indices (NDVI and EVI) and GPP_{EC} for the individual growing season were evaluated. The result shows that NDVI explained over 50%, and EVI explained over 70%, of GPP variance (Table 2). However, NDVI and EVI accounted for only 11% and 30% of GPP variance in 2006 at the Fermi site. This was because the field was infested and dominated by white sweet clover that year, and coverage of other areas that were not much affected by the clover in the MODIS pixel could have contributed for the poor correlation between vegetation indices and GPP in 2006. Thus, we thereafter dropped the 2006 growing season for the Fermi site from further analysis. When data were pooled for both growing seasons (Fig. 8), NDVI and EVI accounted for 62% and 75% of the variation in GPP, respectively, at the El Reno control site. Similarly at the El Reno burned site, NDVI and EVI accounted for 62% and 79% of GPP variance, respectively. At the Fermi site, NDVI and EVI explained 54% and 68% of GPP variance, respectively, for the combined 2005 and 2007 growing seasons (excluding 2006). The results showed that EVI had a stronger linear relationship with GPP than did NDVI.

3.4. Seasonal dynamics of GPP_{VPM} and GPP_{EC}

Seasonal dynamics of modeled GPP (GPP_{VPM}) and GPP_{EC} are compared in Fig. 9. The result shows that the seasonal dynamics of GPP_{VPM} agreed reasonably well with the dynamics of GPP_{EC} at all sites. Both GPP_{EC} and GPP_{VPM} increased rapidly with the beginning of the growing season, reached a maximum during the peak growth period, and declined with the beginning of plant senescence. The seasonal peaks of GPP_{VPM} also match the seasonal peaks of GPP_{EC}.

Simple linear regression models showed good agreement between GPP_{VPM} and GPP_{EC}, and explained a significant amount of variation in GPP at all sites (Table 3). The results show that VPM slightly underestimated GPP at all sites (slopes were 0.89–0.98) in most years (Table 3). Some large discrepancies between GPP_{EC} and GPP_{VPM} were also observed. GPP_{VPM} explained 83% and 75% of the variation in GPP_{EC} for the El Reno control and burned sites in 2005, respectively. But it explained 70% of the variation for the control site and 44% of variation for the burned site in 2006, the drought year, when the original W_{scalar} estimation approach (Eq. (13)) was used. For the Fermi site, GPP_{VPM} accounted for 65% and 80% of the variation in GPP_{EC} in 2005 and 2007, respectively. RMSE and MAE values for the Fermi site were 2.03 and 1.62 g C m^{-2} in 2005, and 1.63 and 1.32 g C m^{-2} in 2007, respectively.

When we examined the influence of the modified approach of W_{scalar} estimation (as shown in Eq. (14)) on drought events that there were large discrepancies between GPP_{EC} and GPP_{VPM} for both El Reno sites in 2006, VPM performance improved greatly (Tables 3 and 4). For example, the R^2 value for the simple linear regression between GPP_{EC} and GPP_{VPM} for the El Reno burned site in 2006 increased from 0.44 to 0.91 (Table 3), and overestimation of GPP dropped to 11% from 38% (Table 4). Similarly, RMSE and MAE dropped from 2.04 to 1.01 g C m^{-2} and from 1.49 to 0.80 g C m^{-2}, respectively (Table 4).

Seasonally integrated GPP_{VPM} over the growing season in 2005 and 2006 for the El Reno control site was 1311 and 757 g C m^{-2}, respectively, while the seasonally integrated GPP_{EC} was 1295 and 842 g C m^{-2}, respectively (Table 4). Table 4 shows that seasonally integrated GPP_{VPM} over the growing season was similar in 2005 and 10% lower in 2006 than the GPP_{EC} at the El Reno control site. At the El Reno burned site,

Table 2
Comparison of simple linear regression models between vegetation indices [normalized difference vegetation index (NDVI) and enhanced vegetation index (EVI)] and tower gross primary production (GPP_{EC}) during the active growing season (GPP > 1 g C m^{-2} day^{-1}) at three tallgrass prairie flux sites.

Site	Growing season	NDVI and GPP_{EC} (R^2 value)	EVI and GPP_{EC} (R^2 value)
El Reno control	2005	0.60	0.69
	2006	0.61	0.75
El Reno burned	2005	0.54	0.72
	2006	0.52	0.76
Fermi prairie	2005	0.43	0.65
	2006	0.11	0.30
	2007	0.57	0.71

seasonally integrated GPP_{VPM} was similar to total GPP_{EC} (1513 g C m^{-2}) and 11% higher than the total GPP_{EC} (734 g C m^{-2}) over the 2005 and 2006 growing seasons, respectively. Similarly, the sum of GPP_{VPM} was 4% lower than the sums of the GPP_{EC} for the Fermi site in the 2005 and 2007 growing seasons.

3.5. MODIS GPP ($GPP_{MOD17A2}$) and tower GPP (GPP_{EC})

$GPP_{MOD17A2}$ was regressed with GPP_{EC} to quantify the correlation between them. Linear regression coefficients are provided in Table 3. $GPP_{MOD17A2}$ explained 39% and 45% of the variation in GPP_{EC} for the El Reno control and burned sites in 2005, respectively. However, $GPP_{MOD17A2}$ explained only 10–12% of the variability in GPP_{EC} for these sites in the dry year (2006). The results show that $GPP_{MOD17A2}$ was substantially lower compared to GPP_{EC} (slopes were 0.30–0.41). $GPP_{MOD17A2}$ data were not available for the Fermi site because the MOD17 algorithm uses MODIS Land Cover Type product (MCD12Q1) as input and the Fermi site is classified as urban or built-up category.

4. Discussion

Strong correspondence between seasonal patterns of the MODIS-derived vegetation indices (EVI, NDVI, and LSWI) and GPP_{EC} indicated the potential of vegetation indices for identifying tallgrass prairie phenology. However, vegetation indices showed slightly weaker relationships with GPP_{EC} at the Fermi site compared to the El Reno sites (Fig. 8). This was because the MODIS pixel at the Fermi site included the strips of corn/soybean rotation and grasslands east of the flux tower, as the fetch to the east was not sufficient (<300 m). As in several previous studies (Jin et al., 2013; Kalfas et al., 2011; Xiao, Hollinger, et al., 2004), we observed a stronger linear relationship between EVI and GPP_{EC} than between NDVI and GPP_{EC} (Fig. 8, Table 2). This finding showed that EVI was more sensitive to changes in GPP_{EC} than was

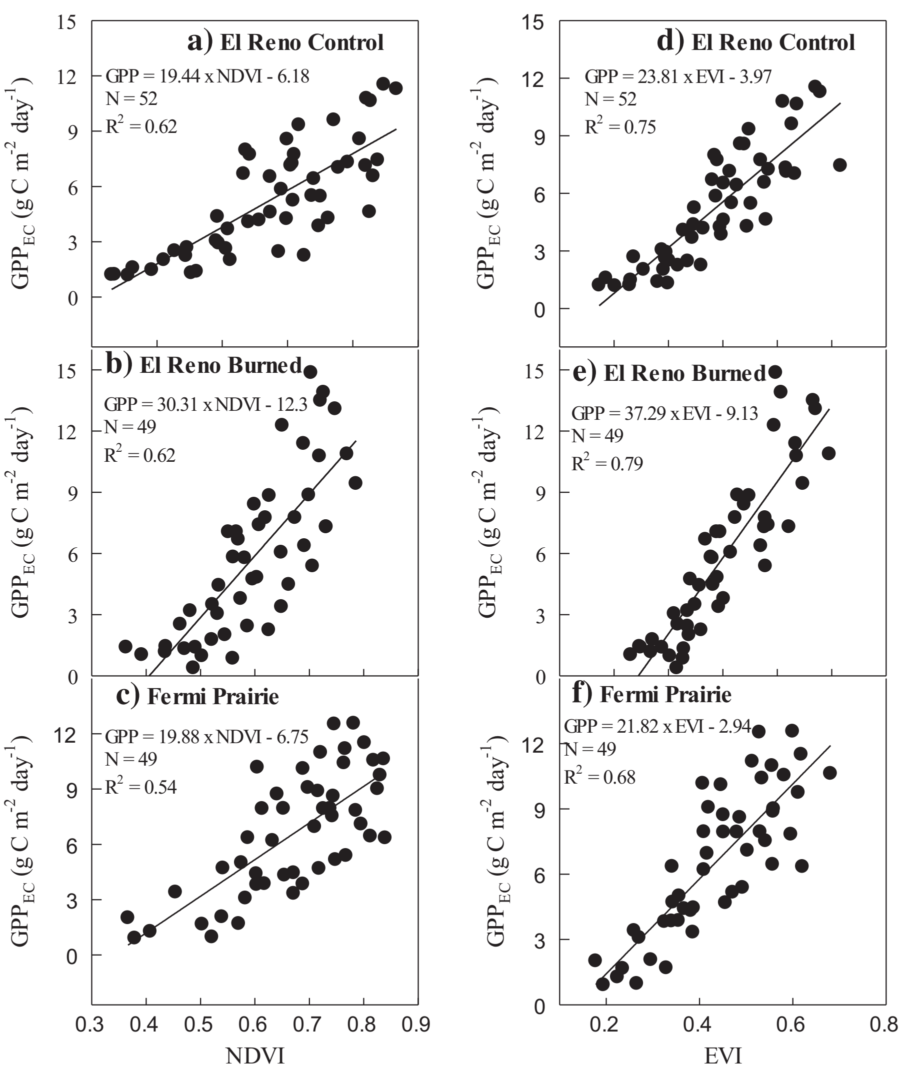

Fig. 8. Comparison of simple linear regression models between vegetation indices (normalized difference vegetation index, NDVI, and enhanced vegetation index, EVI) and gross primary production (GPP_{EC}) during the active growing season (GPP > 1 g C m^{-2} day^{-1}) at three eddy flux sites. Simple linear regression models were highly significant (P < 0.0001).

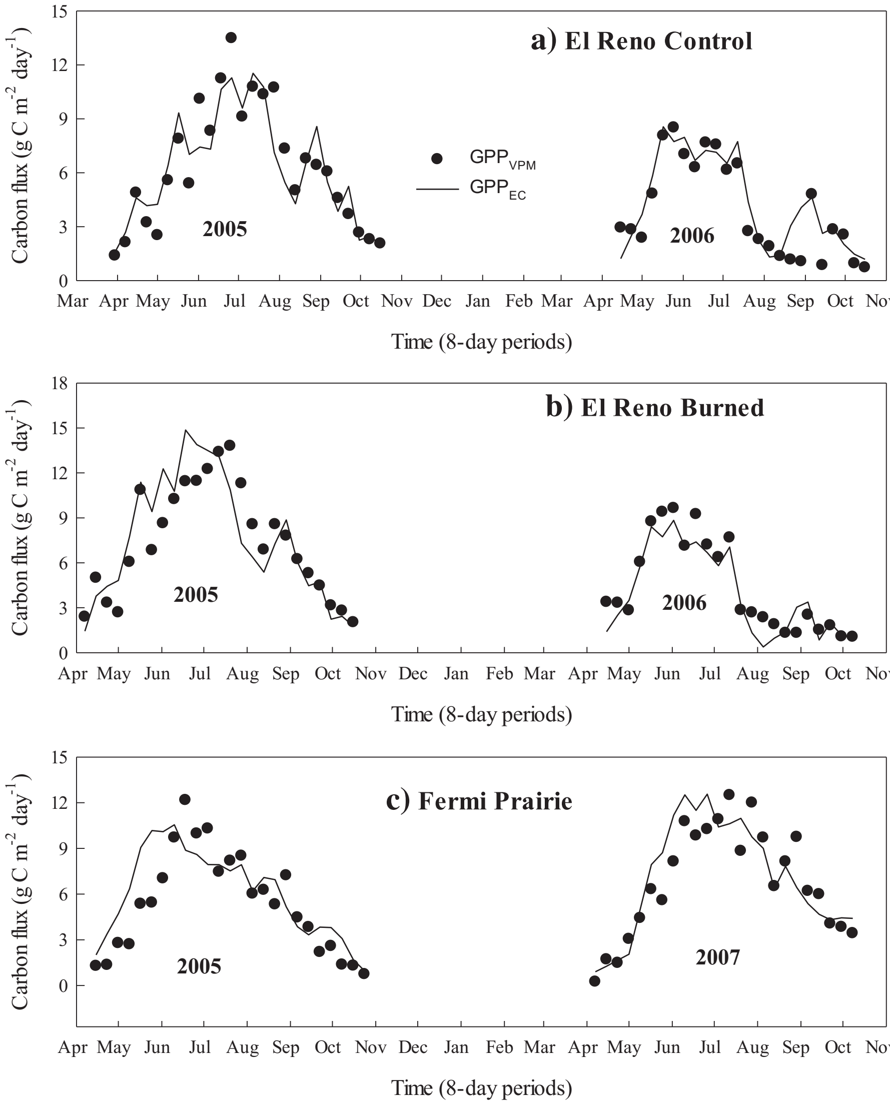

Fig. 9. A comparison of the seasonal dynamics and interannual variations of 8-day composite values of observed gross primary production (GPP_{EC}) and modeled GPP (GPP_{VPM}) at three tallgrass prairie sites.

NDVI. For example, the maximum GPP was 11.5 g C m^{-2} day^{-1} in 2005 and 8.5 g C m^{-2} day^{-1} in 2006 (26% drop), while similar values (0.5% drop) of maximum NDVI (0.77 in 2005 and 0.73 in 2006) were observed in both years at the El Reno control site. But EVI showed a larger reduction (~23% drop) in 2006 (maximum EVI = 0.48) as compared to 2005 (maximum EVI = 0.62). As a result, EVI performed better in tracking the changes in carbon uptake than did NDVI.

NDVI has been the most widely used index for remote sensing of vegetation over the last two decades. It has been used in many applications, including net primary production (NPP) estimations [Carnegie-Ames-

Table 3
Linear regression coefficients and coefficient of determination (R^2) of MOD17A2-based GPP ($GPP_{MOD17A2}$) and vegetation photosynthesis model based estimates of GPP (GPP_{VPM}) with tower GPP (GPP_{EC}) for three tallgrass prairie sites. Two different approaches (Eqs. (13) and (14)) of W_{scalar} (a down-regulation scalar to account for the effect of water stress on light use efficiency) calculation was used for normal and drought periods. Slope and R^2 value in brackets () represent the results when only Eq. (13) was used to determine W_{scalar}. $GPP_{MOD17A2}$ was not available for the Fermi site.

		$GPP_{VPM} = a \times GPP_{EC}$		$GPP_{MOD17A2} = a \times GPP_{EC}$	
Site	Year	Slope	R^2	Slope	R^2
El Reno control	2005	1.01	0.83	0.41	0.39
	2006	0.91 (0.99)	0.85 (0.70)	0.30	0.12
	2005–06	0.98 (1.0)	0.86 (0.81)	0.37	0.40
El Reno burned	2005	0.94	0.75	0.36	0.45
	2006	1.08 (1.17)	0.91 (0.44)	0.33	0.10
	2005–06	0.97 (0.99)	0.84 (0.65)	0.36	0.5
Fermi prairie	2005	0.89	0.65		
	2007	0.94	0.80		
	2005 and 2007	0.92	0.74		

Table 4
Seasonally integrated sums of modeled and tower based gross primary production (GPP, g C m^{-2}), root mean square error (RMSE, g C m^{-2} day^{-1}), and mean absolute error (MAE, g C m^{-2} day^{-1}) for three tallgrass prairie sites. Two different approaches (Eqs (13) and (14)) of W_{scalar} (a down-regulation scalar to account for the effect of water stress on light use efficiency) calculation was used for normal and drought periods. GPP_{VPM}, MAE, and RMSE values in brackets ( ) represent results when only Eq. (13) was used to determine W_{scalar}. The length of the growing season represents the period of GPP > 1 g C m^{-2} day^{-1}.

Site	Period	GPP_{VPM} (g C m^{-2})	GPP_{EC} (g C m^{-2})	MAE (g C m^{-2})	RMSE (g C m^{-2})
El Reno control	Mar 30–Oct 16, 2005	1311	1295	1.07	1.38
	Apr 15–Oct 24, 2006	757 (884)	842	0.83 (0.95)	1.09 (1.27)
El Reno burned	Apr 5–Oct 16, 2005	1482	1513	1.44	1.83
	Apr 15–Oct 16, 2006	817 (1013)	734	0.80 (1.49)	1.01 (2.04)
Fermi Prairie	Apr 15–Oct 24, 2005	1085	1232	1.62	2.03
	Apr 7–Oct 8, 2007	1308	1359	1.32	1.63

Stanford Approach, CASA (Potter et al., 1993)], GPP estimations [Terrestrial Uptake and Release of Carbon, TURC (Ruimy, Dedieu, & Saugier, 1996), GLObal Production Efficiency Model, GLO-PEM (Prince & Goward, 1995), MODIS Photosynthesis, MODIS-PSN (Running, Nemani, Glassy, & Thornton, 1999)], estimation of crop yields (Quarmby, Milnes, Hindle, & Silleos, 1993), and drought monitoring (Peters et al., 2002). Our results indicate that EVI could be a better index for remote-sensing-based applications, especially for regions or time periods with low rates of precipitation.

To link the seasonal dynamics of GPP and EVI with major environmental drivers, we plotted air temperature, vapor pressure deficit (VPD), GPP, and EVI for the El Reno burned site (Fig. 10). Temperature and VPD were higher in 2006 compared to 2005. Canopy CO_2 exchanges increase rapidly with the increasing temperature and VPD in the lower temperature and VPD ranges to reach a maximum, and decrease as temperature and VPD increase beyond a certain threshold (Wagle & Kakani, 2014a). During mid-July to mid-August 2006, 8-day composite air temperature reached up to 31 °C, with the maximum VPD 2.5 kPa. Higher temperature and VPD caused a reduction in both GPP and EVI, but GPP decreased more rapidly than EVI (Fig. 10b), suggesting that GPP was more sensitive to drought than did EVI. A short-period severe drought may not significantly affect EVI, but can limit GPP greatly, because of the stomatal closure control of photosynthesis at high VPD. Previous studies also have suggested that GPP is more sensitive to drought, which in turn was more sensitive than ER (Shurpali, Verma, Kim, & Arkebauer, 1995; Wagle & Kakani, 2013) and evapotranspiration (Wagle & Kakani, 2014b). Light-saturated GPP and daytime averaged canopy conductance decreased up to 90% under drought conditions at Mediterranean evergreen sites (Reichstein et al., 2002).

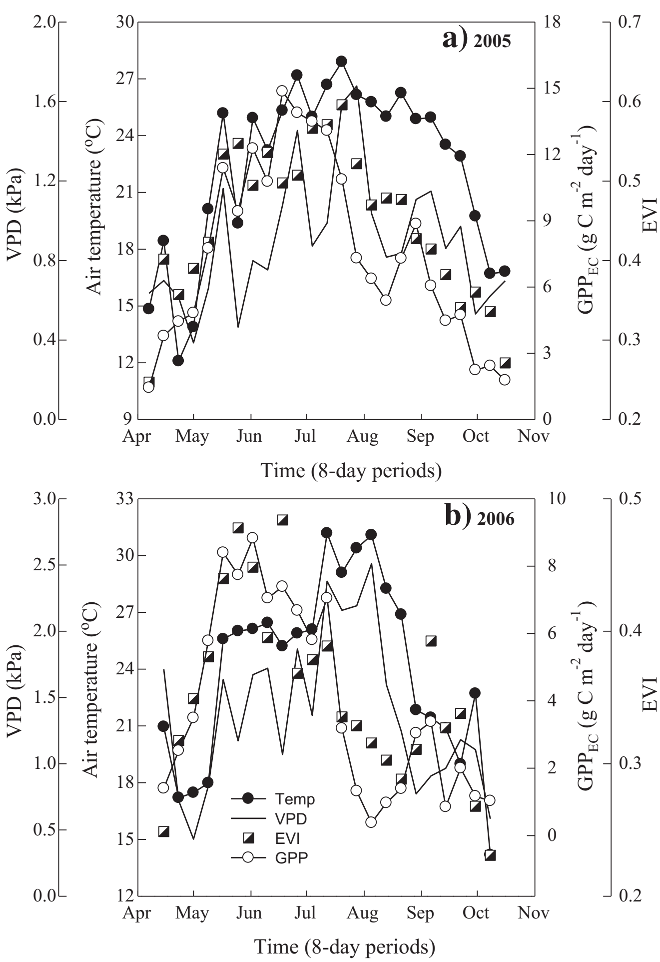

Fig. 10. Seasonal dynamics of air temperature, vapor pressure deficit (VPD), gross primary production (GPP_{EC}), and enhanced vegetation index (EVI) during the 2005 and 2006 growing seasons for the El Reno burned site.

From the characterization of the seasonal evolution of the MODIS-derived LSWI for both El Reno sites, based on 13 years of available data, we found that LSWI values were positive throughout the entire growing season in normal years, but the values dropped below zero during severe droughts, as shown in Fig. 6. This result indicates that LSWI may be used as an indicator to track drought. At both El Reno sites, EVI and LSWI showed a very strong correlation (r > 0.9) during the growing season (May–September). However, the ratio of EVI to LSWI altered greatly in 2006 (drought year), while it did not change much in 2005 at both El Reno sites (Fig. S1), indicating the different responses of EVI and LSWI to drought. When W_{scalar} was modified as shown in Eq. (14) to account for severe drought, VPM performance improved greatly in 2006 for both El Reno sites, yielding higher R^2 values, and smaller MAE and RMSE values (Tables 2 and 3). This is because drought, high temperature, and high VPD are tightly linked to each other. This modification of W_{scalar} for the severe drought period helped to account for the reduction in GPP during periods of higher temperature and VPD.

Simulations by VPM of the six site-years showed good agreement between GPP_{VPM} and GPP_{EC}; seasonally integrated GPP_{VPM} ranged from −5% to +5% of integrated GPP_{EC} in most cases (Tables 3 and 4, Fig. 9). Some discrepancies between GPP_{VPM} and GPP_{EC} can be attributed to prediction error in VPM and estimation error or uncertainty in EC measurements. There are a number of inherent errors/uncertainties in EC measurements, and sources of uncertainties can be attributed to systematic and random errors (Moncrieff, Malhi, & Leuning, 1996). Errors due to the EC instrument system and due to stochastic nature of turbulence, and uncertainty due to changes in footprint can be categorized into random errors (Mauder et al., 2013). Systematic errors include errors resulting from data processing, instrument calibration, and unmet assumptions and methodological challenges (Mauder et al., 2013). Numerous uncertainties are associated with gap filling of eddy flux time series data (Richardson & Hollinger, 2007). Since eddy towers do not provide direct measurements of GPP, the partitioning of NEE into GPP and ER also introduces substantial uncertainties (Hagen et al., 2006). In some cases, GPP underestimation by VPM can be attributed to lower input PAR values during cloudy periods. In fact, LUE increases under cloudy conditions (Turner, Urbanski, et al., 2003). Inclusion of the corn/soybean strip in the MODIS pixel likely contributed to part of the GPP disparity in the Fermi site. Large discrepancies between GPP_{VPM} and GPP_{EC} in 2006 for both El Reno sites (using the original version of W_{scalar} estimation as in Eq. (13)) can be attributed to a severe drought in 2006. Both years of the study period (2005 and 2006) received subnormal precipitation, which led to even drier soils and greater VPDs in 2006. $GPP_{MOD17A2}$ also explained only 10% of the variability in GPP_{EC} at this site in the 2006 growing season, while it explained 45% of the variability in GPP_{EC} during the 2005 growing season. These results indicate the inadequacy of PEM in accounting for the limitation of drought on GPP.

To analyze the response of CO_2 flux to VPD, we examined the diurnal courses of NEE and VPD across the active growing periods (May–August) within the 2005 and 2006 growing seasons for the El Reno burned site (Fig. 11). The diurnal peak value (monthly average) of VPD did not exceed 2.5 kPa in 2005, but in 2006 it reached up to 2.9 kPa in June, 3.9 kPa in July, and 3.5 kPa in August. As a result, NEE showed symmetric diurnal NEE cycles in 2005, with a peak NEE in the afternoon (2–3 PM) when the maximum radiation occurred. In contrast, NEE reached a maximum in the morning hours before radiation reached a peak due to the limitation of high VPD on photosynthesis, and asymmetric diurnal NEE cycles (reduction in NEE rates from morning to afternoon hours at similar light levels) were observed at higher VPD (>3 kPa). A previous study also reported that VPD > 3.5 kPa constrained photosynthesis in tallgrass prairie and the ecosystem was a source of carbon even during the daytime in north-central Oklahoma (Suyker & Verma, 2001). Our study indicates that the large discrepancy between GPP_{VPM} and GPP_{EC} in drought conditions can be attributed to the inability of the model to account for this NEE hysteresis (asymmetric diurnal patterns of NEE).

It is worth mentioning that satellite-based models use 8-day averaged values of environmental variables. Our observation shows that 8-day averaged values cannot account for short-term extreme climate events. For example, observation of half-hourly values shows that temperature reached up to 40 °C, and VPD reached a maximum of 5.8 kPa, for the El Reno sites in 2006. But observation of 8-day averaged values shows that temperature reached a maximum of 31 °C, with the maximum VPD 2.5 kPa. From the analysis of half-hourly flux measurements, we demonstrated that temperature around 30 °C is optimal for GPP in tallgrass prairie (Fig. 4), and photosynthesis was unaffected up to VPD of 3 kPa (Fig. 11). VPM was thus unable to account for the reduction in photosynthesis even in warm and dry periods. Our results indicate that the use of 8-day averaged VPD values may not be helpful, even though a number of PEM [3-PG (Law, Anthoni, & Aber, 2000), GLO-PEM (Prince & Goward, 1995), MODIS-PSN (Running, Nemani, Glassy, & Thornton, 1999)] use VPD for the LUE calculation. This finding suggests that the PEM simulation results could be improved, especially under unfavorable climatic conditions, if the models were run at hourly or daily scales.

$GPP_{MOD17A2}$ was substantially lower than GPP_{EC} at both El Reno sites (Fig. 12), while the magnitude of GPP_{VPM} was similar to that of GPP_{EC} (Fig. 9). VPM uses meteorological data from flux sites while MODIS-GPP algorithm (MODIS-PSN) uses global climate data. Thus, a better performance of VPM may partly be attributed to the local input data. VPM estimates GPP based on PAR, EVI, and LUE (Eq. (9)) as $fAPAR_{chl}$ is estimated with EVI. From a biochemical perspective, vegetation canopies are composed of photosynthetic and nonphotosynthetic vegetation, and correspondingly the $FPAR_{canopy}$ (FPAR%) is partitioned into $FPAR_{chl} + FPAR_{npv}$. $FPAR_{canopy}$ should be larger than the $FPAR_{chl}$ (=EVI

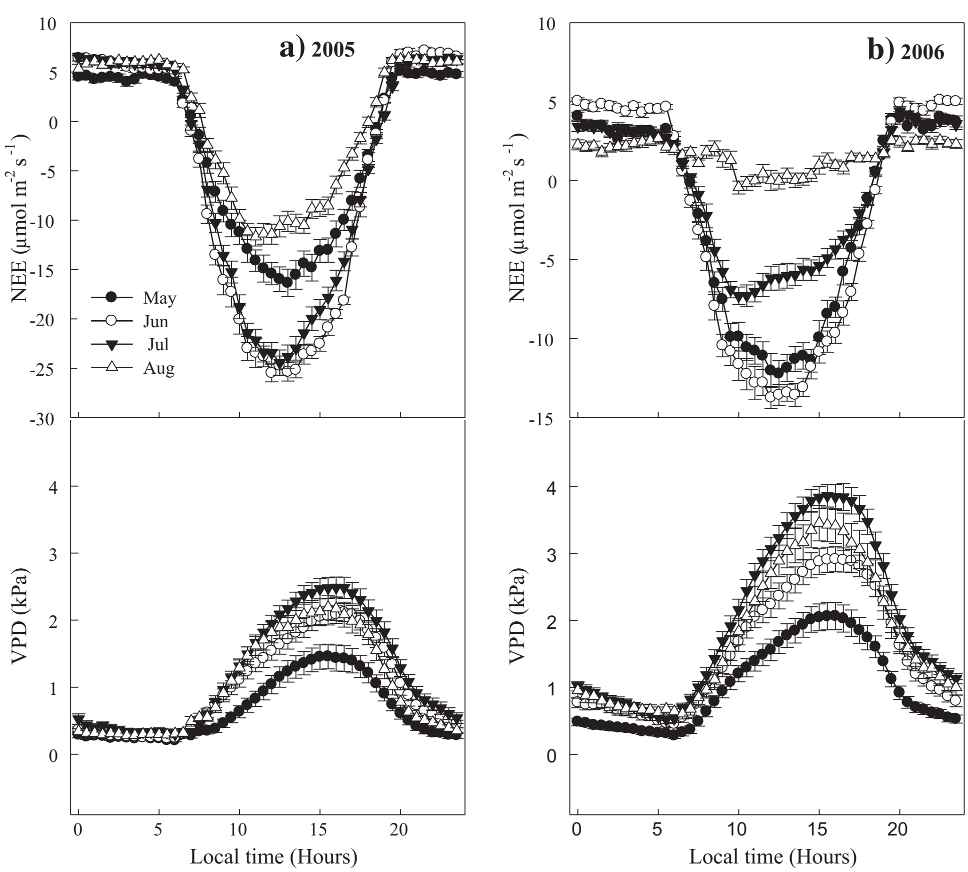

Fig. 11. Half-hourly binned diurnal courses of net ecosystem CO_2 exchange (NEE) and vapor pressure deficit (VPD) for May to August during the 2005 and 2006 growing seasons at the El Reno burned site. Negative values of NEE indicate net carbon uptake and positive values indicate carbon release by the ecosystem. Each data point is a mean value for the specific time step for the entire month and bars represent standard errors of the means.

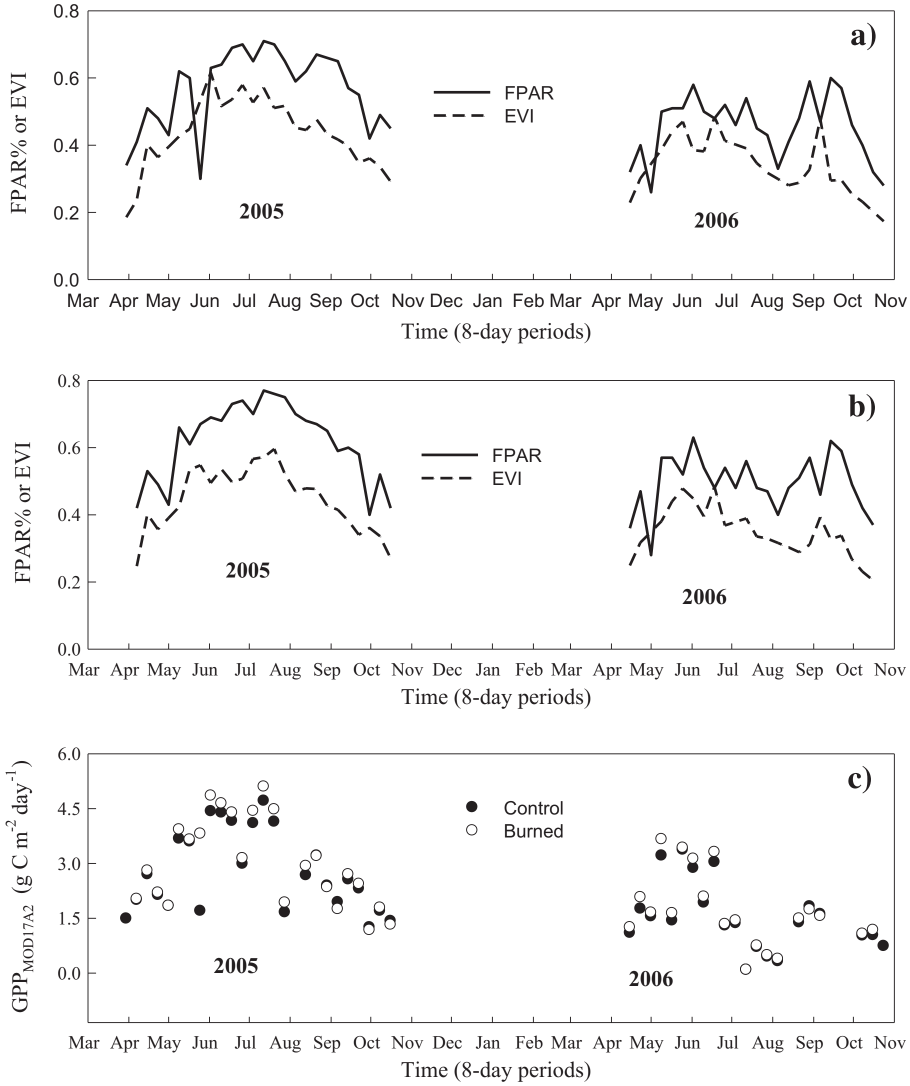

Fig. 12. Comparison of MODIS-derived fraction of absorbed radiation by canopy (FPAR%) and enhanced vegetation index (EVI) at the El Reno control (a) and burned (b) sites for the 2005 and 2006 growing seasons. MODIS GPP ($GPP_{MOD17A2}$) for the 2005 and 2006 growing seasons is shown for the El Reno control and burned sites (c).

in VPM), which is supported by Fig. 12. Fig. 12 shows that $FPAR_{canopy}$ was consistently larger than EVI over the entire growing seasons at both sites. It indicates that a model using $FPAR_{canopy}$ in GPP calculations may overestimate GPP. However, $GPP_{MOD17A2}$ was substantially lower than GPP_{VPM}. This result indicates that underestimation of $GPP_{MOD17A2}$ is associated with the smaller ε parameter. A single ε value per biome type is used in the standard MODIS-GPP algorithm (MOD17A2), based on the assumption that biome-specific physiological parameters do not vary with space or time. However, several studies have shown that the LUE in fact varies widely between biome types and in response to environmental conditions (Gower, Kucharik, & Norman, 1999; Scott Green, Erickson, & Kruger, 2003). The value of ε used in the MOD17A2 algorithm for grassland is 0.68 g C MJ^{-1} PPFD (~0.15 g C mol^{-1} PPFD, with an approximate conversion factor of 4.6 between MJ PPFD and mol PPFD), which is much smaller than 0.9 g C mol^{-1} PPFD used in VPM in this study. Use of a single LUE_{max} value of 0.9 g C mol^{-1} PPFD in VPM was able to model GPP across multiple sites and multiple years in this study, because VPM employs down-regulation scalars, T_{scalar} and W_{scalar}, to account for the effects of temperature and water on the LUE, respectively. It is important to note that selection of LUE values greatly impacts the accuracy of the models, and that estimation of LUE has been problematic, since it varies with biome types and environmental conditions. In a long term replicated experiment of loblolly and slash pine stands, LUE varied by a factor of two over spatial and temporal scales, with changes in soil nutrient availability and stand development (Martin & Jokela, 2004). Thus, LUE values need to be calibrated rigorously for LUE-based PEM. More studies are needed to better quantify LUE values across varying vegetation types and weather conditions, which will in turn provide greater insight into the uncertainty of PEMs. The use of a constant maximum value of LUE for estimating GPP in the LUE-based PEM also introduces some biases since the use of one single value of LUE for a biome type represents the mean conditions for a particular type of vegetation and it cannot appropriately reflect the contribution of shaded leaves to GPP (Zhang et al., 2012).

5. Conclusions

We used eddy flux CO_2 data at three tallgrass prairie sites for a total of six site-years to validate modeled GPP dynamics using a satellite-based VPM. The eddy flux measurements showed that this ecosystem has distinct spatial and temporal dynamics in GPP. However, our result illustrates the potential of MODIS-derived vegetation indices and VPM to track seasonal dynamics and interannual variations in GPP of tallgrass prairie. On a growing season basis, the modeled GPP totals were generally within $\pm 5\%$ of the measured values. However, larger discrepancies between GPP_{VPM} and GPP_{EC} occurred during noticeable dry spells as GPP was more sensitive to drought than were vegetation indices. This study indicates the necessity of incorporating the effects of extreme climate events on GPP into PEMs to be able to capture the rapid rise or fall in GPP. Development of a modified W_{scalar} function to account for the substantial reduction in GPP during droughts improved VPM's performance to estimate GPP. The use of 8-day averaged values smooth out the effect of short-term extreme climate events, suggesting that satellite-based models should be run at hourly or daily intervals to account for the effects of extreme climate events.

Supplementary data to this article can be found online at http://dx.doi.org/10.1016/j.rse.2014.05.010.

Acknowledgements

This study was supported in part by a research grant (Project No. 2012-02355) through the USDA National Institute for Food and Agriculture (NIFA)'s Agriculture and Food Research Initiative (AFRI), Regional Approaches for Adaptation to and Mitigation of Climate Variability and Change, and a research grant from the National Science Foundation EPSCoR (IIA-1301789). We would also like to thank Melissa L. Scott and Dan Hawkes for the English correction and manuscript editing. We thank two reviewers for their critiques and suggestions on the earlier version of the manuscript.

References

Baldocchi, D., Falge, E., Gu, L., Olson, R., Hollinger, D., Running, S., et al. (2001). FLUXNET: A new tool to study the temporal and spatial variability of ecosystem-scale carbon dioxide, water vapor, and energy flux densities. *Bulletin of the American Meteorological Society*, *82*, 2415–2434.

Beer, C., Reichstein, M., Tomelleri, E., Ciais, P., Jung, M., Carvalhais, N., et al. (2010). Terrestrial gross carbon dioxide uptake: Global distribution and covariation with climate. *Science*, *329*, 834–838.

Falge, E., Baldocchi, D., Tenhunen, J., Aubinet, M., Bakwin, P., Berbigier, P., et al. (2002). Seasonality of ecosystem respiration and gross primary production as derived from FLUXNET measurements. *Agricultural and Forest Meteorology*, *113*, 53–74.

Field, C. B., Randerson, J. T., & Malmström, C. M. (1995). Global net primary production: Combining ecology and remote sensing. *Remote Sensing of Environment*, *51*, 74–88.

Fischer, M. L., Torn, M. S., Billesbach, D. P., Doyle, G., Northup, B., & Biraud, S. C. (2012). Carbon, water, and heat flux responses to experimental burning and drought in a tallgrass prairie. *Agricultural and Forest Meteorology*, *166*, 169–174.

Gower, S. T., Kucharik, C. J., & Norman, J. M. (1999). Direct and indirect estimation of leaf area index, f_{APAR}, and net primary production of terrestrial ecosystems. *Remote Sensing of Environment*, *70*, 29–51.

Hagen, S., Braswell, B., Linder, E., Frolking, S., Richardson, A., & Hollinger, D. (2006). Statistical uncertainty of eddy flux-based estimates of gross ecosystem carbon exchange at Howland Forest, Maine. *Journal of Geophysical Research, [Atmospheres]*, *111*, D08S03.

He, H., Liu, M., Xiao, X., Ren, X., Zhang, L., Sun, X., et al. (2014). Large-scale estimation and uncertainty analysis of gross primary production in Tibetan alpine grasslands. *Journal of Geophysical Research — Biogeosciences*, *2013*, JG002449.

Huete, A., Liu, H., Batchily, K., & Van Leeuwen, W. (1997). A comparison of vegetation indices over a global set of TM images for EOS-MODIS. *Remote Sensing of Environment*, *59*, 440–451.

Jin, C., Xiao, X., Merbold, L., Arneth, A., Veenendaal, E., & Kutsch, W. L. (2013). Phenology and gross primary production of two dominant savanna woodland ecosystems in Southern Africa. *Remote Sensing of Environment*, *135*, 189–201.

Kalfas, J. L., Xiao, X., Vanegas, D. X., Verma, S. B., & Suyker, A. E. (2011). Modeling gross primary production of irrigated and rain-fed maize using MODIS imagery and CO_2 flux tower data. *Agricultural and Forest Meteorology*, *151*, 1514–1528.

Law, B., Anthoni, P., & Aber, J. (2000). Measurements of gross and net ecosystem productivity and water vapour exchange of a *Pinus ponderosa* ecosystem, and an evaluation of two generalized models. *Global Change Biology*, *6*, 155–168.

Li, Z., Yu, G., Xiao, X., Li, Y., Zhao, X., Ren, C., et al. (2007). Modeling gross primary production of alpine ecosystems in the Tibetan Plateau using MODIS images and climate data. *Remote Sensing of Environment*, *107*, 510–519.

Martin, T. A., & Jokela, E. J. (2004). Developmental patterns and nutrition impact radiation use efficiency components in southern pine stands. *Ecological Applications*, *14*, 1839–1854.

Mauder, M., Cuntz, M., Drüe, C., Graf, A., Rebmann, C., Schmid, H. P., et al. (2013). A strategy for quality and uncertainty assessment of long-term eddy-covariance measurements. *Agricultural and Forest Meteorology*, *169*, 122–135.

Moncrieff, J., Malhi, Y., & Leuning, R. (1996). The propagation of errors in long-term measurements of land-atmosphere fluxes of carbon and water. *Global Change Biology*, *2*, 231–240.

Monteith, J. (1972). Solar radiation and productivity in tropical ecosystems. *Journal of Applied Ecology*, *9*, 747–766.

Myneni, R., Hoffman, S., Knyazikhin, Y., Privette, J., Glassy, J., Tian, Y., et al. (2002). Global products of vegetation leaf area and fraction absorbed PAR from year one of MODIS data. *Remote Sensing of Environment*, *83*, 214–231.

Papale, D., & Valentini, R. (2003). A new assessment of European forests carbon exchanges by eddy fluxes and artificial neural network spatialization. *Global Change Biology*, *9*, 525–535.

Peters, W., Jacobson, A. R., Sweeney, C., Andrews, A. E., Conway, T. J., Masarie, K., et al. (2007). An atmospheric perspective on North American carbon dioxide exchange: CarbonTracker. *Proceedings of the National Academy of Sciences*, *104*, 18925–18930.

Peters, A. J., Walter-Shea, E. A., Ji, L., Vina, A., Hayes, M., & Svoboda, M. D. (2002). Drought monitoring with NDVI-based standardized vegetation index. *Photogrammetric Engineering and Remote Sensing*, *68*, 71–75.

Potter, C. S., Randerson, J. T., Field, C. B., Matson, P. A., Vitousek, P. M., Mooney, H. A., et al. (1993). Terrestrial ecosystem production: A process model based on global satellite and surface data. *Global Biogeochemical Cycles*, *7*, 811–841.

Prince, S. D., & Goward, S. N. (1995). Global primary production: A remote sensing approach. *Journal of Biogeography*, *815–835*.

Quarmby, N., Milnes, M., Hindle, T., & Silleos, N. (1993). The use of multi-temporal NDVI measurements from AVHRR data for crop yield estimation and prediction. *International Journal of Remote Sensing*, *14*, 199–210.

Raich, J., Rastetter, E., Melillo, J., Kicklighter, D., Steudler, P., Peterson, B., et al. (1991). Potential net primary productivity in South America: Application of a global model. *Ecological Applications*, *1*, 399–429.

Reichstein, M., Falge, E., Baldocchi, D., Papale, D., Aubinet, M., Berbigier, P., et al. (2005). On the separation of net ecosystem exchange into assimilation and ecosystem respiration: Review and improved algorithm. *Global Change Biology*, *11*, 1424–1439.

Reichstein, M., Tenhunen, J. D., Roupsard, O., Ourcival, J. -m, Rambal, S., Miglietta, F., et al. (2002). Severe drought effects on ecosystem CO_2 and H_2O fluxes at three Mediterranean evergreen sites: Revision of current hypotheses? *Global Change Biology*, *8*, 999–1017.

Richardson, A. D., & Hollinger, D. Y. (2007). A method to estimate the additional uncertainty in gap-filled NEE resulting from long gaps in the CO_2 flux record. *Agricultural and Forest Meteorology*, *147*, 199–208.

Ruimy, A., Dedieu, G., & Saugier, B. (1996). TURC: A diagnostic model of continental gross primary productivity and net primary productivity. *Global Biogeochemical Cycles*, *10*, 269–285.

Ruimy, A., Jarvis, P., Baldocchi, D., & Saugier, B. (1995). CO_2 fluxes over plant canopies and solar radiation: A review. *Advances in Ecological Research*, *26*, 1–68.

Ruimy, A., Kergoat, L., & Bondeau, A. (1999). Comparing global models of terrestrial net primary productivity (NPP): Analysis of differences in light absorption and light-use efficiency. *Global Change Biology*, *5*, 56–64.

Ruimy, A., Saugier, B., & Dedieu, G. (1994). Methodology for the estimation of terrestrial net primary production from remotely sensed data. *Journal of Geophysical Research, [Atmospheres]*, *99*, 5263–5283.

Running, S., Baldocchi, D., Turner, D., Gower, S., Bakwin, P., & Hibbard, K. (1999). A global terrestrial monitoring network integrating tower fluxes, flask sampling, ecosystem modeling and EOS satellite data. *Remote Sensing of Environment*, *70*, 108–127.

Running, S. W., Nemani, R., Glassy, J. M., & Thornton, P. E. (1999). *MODIS daily photosynthesis (PSN) and annual net primary production (NPP) product (MOD17)*. Algorithm Theoretical Basis Document Version 3.0.

Schmid, H. (1994). Source areas for scalars and scalar fluxes. *Boundary-Layer Meteorology*, *67*, 293–318.

Scott Green, D., Erickson, J. E., & Kruger, E. L. (2003). Foliar morphology and canopy nitrogen as predictors of light-use efficiency in terrestrial vegetation. *Agricultural and Forest Meteorology*, *115*, 163–171.

Shurpali, N., Verma, S., Kim, J., & Arkebauer, T. (1995). Carbon dioxide exchange in a peatland ecosystem. *Journal of Geophysical Research*, *100*(14319–14314), 14326.

Suyker, A. E., & Verma, S. B. (2001). Year-round observations of the net ecosystem exchange of carbon dioxide in a native tallgrass prairie. *Global Change Biology*, *7*, 279–289.

Suyker, A. E., Verma, S. B., & Burba, G. G. (2003). Interannual variability in net CO_2 exchange of a native tallgrass prairie. *Global Change Biology*, *9*, 255–265.

Tucker, C. J. (1979). Red and photographic infrared linear combinations for monitoring vegetation. *Remote Sensing of Environment*, *8*, 127–150.

Turner, D. P., Ritts, W. D., Cohen, W. B., Gower, S. T., Zhao, M., Running, S. W., et al. (2003). Scaling gross primary production (GPP) over boreal and deciduous forest landscapes in support of MODIS GPP product validation. *Remote Sensing of Environment*, *88*, 256–270.

Turner, D. P., Urbanski, S., Bremer, D., Wofsy, S. C., Meyers, T., Gower, S. T., et al. (2003). A cross-biome comparison of daily light use efficiency for gross primary production. *Global Change Biology*, *9*, 383–395.

Verma, S. B., Kim, J., & Clement, R. J. (1989). Carbon dioxide, water vapor and sensible heat fluxes over a tallgrass prairie. *Boundary-Layer Meteorology*, *46*, 53–67.

Wagle, P., & Kakani, V. G. (2013). Seasonal variability in net ecosystem carbon dioxide exchange over a young Switchgrass stand. *GCB Bioenergy*. http://dx.doi.org/10.1111/gcbb.12049.

Wagle, P., & Kakani, V. G. (2014a). Environmental control of daytime net ecosystem exchange of carbon dioxide in switchgrass. *Agriculture, Ecosystems & Environment*, *186*, 170–177.

Wagle, P., & Kakani, V. G. (2014b). Growing season variability in evapotranspiration, ecosystem water use efficiency, and energy partitioning in switchgrass. *Ecohydrology*, *7*, 64–72.

Wang, Z., Xiao, X., & Yan, X. (2010). Modeling gross primary production of maize cropland and degraded grassland in northeastern China. *Agricultural and Forest Meteorology*, *150*, 1160–1167.

Wu, C., Chen, J. M., & Huang, N. (2011). Predicting gross primary production from the enhanced vegetation index and photosynthetically active radiation: Evaluation and calibration. *Remote Sensing of Environment*, *115*, 3424–3435.
Wu, C., Gonsamo, A., Zhang, F., & Chen, J. M. (2014). The potential of the greenness and radiation (GR) model to interpret 8-day gross primary production of vegetation. *ISPRS Journal of Photogrammetry and Remote Sensing*, *88*, 69–79.
Wu, W., Wang, S., Xiao, X., Yu, G., Fu, Y., & Hao, Y. (2008). Modeling gross primary production of a temperate grassland ecosystem in Inner Mongolia, China, using MODIS imagery and climate data. *Science in China Series D: Earth Sciences*, *51*, 1501–1512.
Xiao, X., Boles, S., Liu, J., Zhuang, D., & Liu, M. (2002). Characterization of forest types in Northeastern China, using multi-temporal SPOT-4 VEGETATION sensor data. *Remote Sensing of Environment*, *82*, 335–348.
Xiao, X., Hollinger, D., Aber, J., Goltz, M., Davidson, E. A., Zhang, Q., et al. (2004). Satellite-based modeling of gross primary production in an evergreen needleleaf forest. *Remote Sensing of Environment*, *89*, 519–534.
Xiao, X., Zhang, Q., Braswell, B., Urbanski, S., Boles, S., Wofsy, S., et al. (2004). Modeling gross primary production of temperate deciduous broadleaf forest using satellite images and climate data. *Remote Sensing of Environment*, *91*, 256–270.
Xiao, X., Zhang, Q., Hollinger, D., Aber, J., & Moore, B., III (2005). Modeling gross primary production of an evergreen needleleaf forest using MODIS and climate data. *Ecological Applications*, *15*, 954–969.
Xiao, X., Zhang, Q., Saleska, S., Hutyra, L., De Camargo, P., Wofsy, S., et al. (2005). Satellite-based modeling of gross primary production in a seasonally moist tropical evergreen forest. *Remote Sensing of Environment*, *94*, 105–122.
Xiao, J., Zhuang, Q., Baldocchi, D. D., Law, B. E., Richardson, A. D., Chen, J., et al. (2008). Estimation of net ecosystem carbon exchange for the conterminous United States by combining MODIS and AmeriFlux data. *Agricultural and Forest Meteorology*, *148*, 1827–1847.
Xiao, J., Zhuang, Q., Law, B. E., Chen, J., Baldocchi, D. D., Cook, D. R., et al. (2010). A continuous measure of gross primary production for the conterminous United States derived from MODIS and AmeriFlux data. *Remote Sensing of Environment*, *114*, 576–591.
Yamaji, T., Sakai, T., Endo, T., Baruah, P. J., Akiyama, T., Saigusa, N., et al. (2008). Scaling-up technique for net ecosystem productivity of deciduous broadleaved forests in Japan using MODIS data. *Ecological Research*, *23*, 765–775.
Zhang, F., Chen, J. M., Chen, J., Gough, C. M., Martin, T. A., & Dragoni, D. (2012). Evaluating spatial and temporal patterns of MODIS GPP over the conterminous US against flux measurements and a process model. *Remote Sensing of Environment*, *124*, 717–729.